J Mater Sci: Mater Med (2015) 26:158
DOI 10.1007/s10856-015-5479-2

Upregulation of cell proliferation via Shc and ERK1/2 MAPK signaling in SaOS-2 osteoblasts grown on magnesium alloy surface coating with tricalcium phosphate

Tianlong Jiang[1] · Lei Guo[1] · Shenghui Ni[1] · Yuyan Zhao[2]

Received: 4 June 2014 / Accepted: 9 February 2015 / Published online: 18 March 2015

Abstract Magnesium (Mg) alloys have been demonstrated to be viable orthopedic implants because of mechanical and biocompatible properties similar to natural bone. In order to improve its osteogenic properties, a porous β-tricalcium phosphate (β-TCP) was coated on the Mg–3AI–1Zn alloy by alkali-heat treatment technique. The human bone-derived cells (SaOS-2) were cultured on (β-TCP)–Mg–3AI–1Zn in vitro, and the osteoblast response, the morphology and the elements on this alloy surface were investigated. Also, the regulation of key intracellular signalling proteins was investigated in the SaOS-2 cells cultured on alloy surface. The results from scanning electron microscope and immunofluorescence staining demonstrated that (β-TCP)–Mg–3AI–1Zn induced significant osteogenesis. SaOS-2 cell proliferation was improved by β-TCP coating. Moreover, the (β-TCP)–Mg–3AI–1Zn surface induced activation of key intracellular signalling proteins in SaOS-2 cells. We observed an enhanced activation of Src homology and collagen (Shc), a common point of integration between bone morphogenetic protein 2, and the Ras/mitogen-activated protein kinase (MAPK) pathway. ERK1/2 MAP kinase activation was also upregulated, suggesting a role in mediating osteoblastic cell interactions with biomaterials. The signalling pathway involving c-fos (member of the activated protein-1) was also shown to be upregulated in osteoblasts cultured on the (β-TCP)–Mg–3AI–1Zn. These results suggest that β-TCP coating may contribute to successful osteoblast function on Mg alloy surface. (β-TCP)–Mg–3AI–1Zn may upregulate cell proliferation via Shc and ERK1/2 MAPK signaling in SaOS-2 osteoblasts grown on Mg alloy surface.

1 Introduction

Magnesium (Mg) alloys have been chosen as biomedical materials due to degradation properties in vivo [1–3] and excellent mechanical properties compared to other metals [4]. Mg alloys have good biocompatibility and osteoconductivity in vivo and in vitro [3, 4], but the high corrosion rate and early inflammatory reaction around implants in vivo have limited the clinical application of these alloys [4, 5]. Therefore, there is a need to develop novel micro-engineered surfaces to provide better biological implants. Recently, various surface treatments have been applied to Mg alloys in an attempt to control its corrosion and enhance bone formation. However, to date, none of these surface treatments has generated an interface stable enough to support bone formation and control degradation of Mg alloys, especially during the early stages of bone formation. Surface modification such as through Al coating [6, 7], Ti coating [8] and heat treatment [9] has been applied to Mg alloys to improve the corrosion resistance. However, surface biocompatibility was not enhanced. Hence, for Mg alloys to be useful in the clinic, there is a need to develop Mg alloys with surface coatings that improves biocompatibility. We propose to improve integration of an implant in bone by altering the interfacial chemistry of biomaterial with bioactive molecules.

✉ Lei Guo
g572@sina.com

[1] Department of Orthopedic Surgery, First Affiliated Hospital, China Medical University, Shenyang 110001, Liaoning, People's Republic of China

[2] Department of Endocrinology, First Affiliated Hospital, China Medical University, Shenyang 110001, Liaoning, People's Republic of China

Calcium–phosphate (Ca–P) coatings have become an interesting topic in the field of bioengineering, due to their favorable biocompatibility [10]. Bioactive coatings using various Ca–P compounds are of importance for modifying the surface of implanted devices [11]. Ca–P coatings have been successfully applied to the surface treatment of Ti and its alloys in order to promote direct attachment of the surrounding bone and to suppress the release of corrosion products into the human body [12, 13]. It is now accepted that bone apatite can be denoted as carbonate hydroxyapatite and approximated by the formula $(Ca,Mg,Na)_{10}(PO_4CO_3)_6(OH)_2$, and its composition is similar to bone mineral apatite [14]. Due to its good chemical stability, relative mechanical strength, and bioabsorption rate [15], β-tricalcium phosphate (β-TCP) coated on Mg alloys might improve the possibility of applying Mg alloys in the clinic [16, 17]. The biological apatites are not pure hydroxyapatite but contain trace elements including Mg and zinc (Zn). Mg deficiency significantly and progressively diminishes bone formation, leading to osteoporosis [18], while Zn stimulates bone formation [19] and its deficiency has been linked to the development of osteoporosis [20].

Bone morphogenetic protein 2 (BMP-2), which is member of the transforming growth factor (TGF)-β superfamily, has profound effects on osteoblast activity [21, 22]. In vitro, BMP-2 increases the colony formation of normal human bone marrow stromal preosteoblasts and induces their differentiation into cells with mature osteoblastic phenotype [23]. In addition to the effects on osteoblast growth and differentiation, both BMP-2 and TGF-β can induce osteoblast chemotaxis, which is essential for bone formation to occur [24]. In osteoblasts, both BMP-2 and TGF-β can stimulate the expression of Smad and c-Fos, an activated protein-1 (AP-1) component [25–28]. Because Ras is the upstream effector of Fos and mitogen-activated protein kinase (MAPK), and AP-1-responsive element is present in the promoters of major bone matrix proteins such as type I collagen, osteocalcin, osteopontin, and fibronectin, the induction of Ras/MAPK/AP-1 appears to be an important signal transduction pathway in mediating some of the effects of BMP-2 and TGF-β in osteoblasts [25–27]. Growth factor (such as epidermal growth factor) signaling binding receptor tyrosine kinase or extracellular matrix binding integrin receptor can activate Ras protein [25, 26]. The activated Ras can start a series of signaling cascades. Activation of the Ras pathway has been associated with cell proliferation and these molecular events may involve osteogenic signals [26, 28]. In addition, MAPK pathway activation has been shown to regulate bone formation. The Ras-MAPK pathway is involved in differentiation of C3H10T/12 cells [28] whereas extracellularly regulated kinases 1/2 (ERK1/2) mediates BMP-2 stimulation of fibronectin and osteopontin [29]. Thus, ERK1/2 MAP kinase and p38 MAP kinase differentially mediate BMP-2 function in osteoblasts. BMP-2 activates multiple cytoskeletal-associated and intracellular signaling proteins, such as Src homology and collagen (Shc) [30]. The Shc-Grb2-complex activates Ras, leading to stimulation of the MAPK signaling cascade [31]. The phosphorylated ERK1/2 translocates to the nucleus, providing a link between cytoplasmic signaling molecules and nuclear proteins. The nuclear target proteins of MAPK include c-fos and members of the activated protein-1(c-jun) [32]. Hence ERK1/2, Shc, c-fos and AP-1 play an important role in bone development [26–31].

Whether activation of intracellular signaling cascade can result from the surface modification of biomaterials remains unknown. Therefore, in this study, we investigated the status of important signaling pathways of bone growth with use of Ca–P coatings and Mg alloys. Our results suggest that the β-TCP-coated Mg alloy may upregulate cell proliferation via Shc and ERK1/2 MAPK signaling in SaOS-2 osteoblasts cultured on Mg alloy surface. The surface-coated Mg alloy with β-TCP may enhance the activity of key signalling proteins in human osteoblasts and that in turn may lead to enhanced protein expression of extracellular matrix factors at the bone cells–implant interface.

2 Methods

2.1 Sample preparation

The surface-coated Mg alloy (Mg–3AI–1Zn) with β-TCP [(β-TCP)–Mg–3AI–1Zn] was generated at the Institute of Metal Research, Chinese Academy of Science, through a phosphating process on the naked Mg–3AI–1Zn. The dimensions for the samples used in the cell biology experiments are 5 mm in diameter and 1 mm in thickness following cutting from cast ingots. Samples were sterilized in epoxyethane for 5 min and dried in air. During the in vitro experiments, the titanium alloy (Ti–6Al–4V) and surface-coated Ti–6Al–4V with β-TCP [(β-TCP)–Ti–6Al–4V] which have the same size were generated by phosphating process and used as control.

2.2 β-TCP coating treatment

Samples were cut from Mg–3AI–1Zn or Ti–6Al–4V cast ingots. The samples were ground and dry polished with SiC papers successively up to 2000 grits. The polished samples were ultrasonically rinsed for 10 min in alcohol, dried in a warm air stream, immersed in a supersaturated Na_2HPO_4 solution at room temperature for 3 h and then subjected to heat-treatment at 400 °C for 10 h. After the alkali and heat

treatments, these were ultrasonically cleaned again in distilled water for 10 min and then placed into the falcon tubes which was filled with a mixture of Na_2HPO_4–$12H_2O$ (23.75 g/L) and $Ca(NO_3)_2$ (18.2 g/L) in deionized water at 70 °C for 48 h. The samples were then washed with distilled water and dried in the air.

2.3 Cells culture

Cell lines SaOS-2 (human osteosarcoma cells) were cultured in a DMEM1640 (Gibco, USA) medium containing 2 mmol/L glutamine, 100 IU/mL penicillin, 100 μg/mL streptomycin sulphate and 10 % (v/v) FBS. Then, the cells were incubated at 37 °C with 5 % CO_2 in a humidified incubator. SaOS-2 Cells were seeded on the naked Mg–3AI–1Zn, Ti–6Al–4V, (β-TCP)–Mg–3AI–1Zn and (β-TCP)–Ti–6Al–4V samples at a cell density of 1×10^5 cell/mL. Cultures were incubated in six well plates for 24 h at 37 °C with 5 % CO_2 in a humidified incubator. Three parallel samples were tested in this experiment. After different incubation periods, the samples were washed three times with phosphate-buffered saline (PBS) to remove non-adherent cells.

2.4 Fluorescence imaging

SaOS-2 cells were cultured with samples for 24 h, fixed in 4.0 % formaldehyde solution for 15 min, and then used for immunofluorescence staining. The distinct differences in the responses of the cells to the different surfaces were visualized under fluorescence microscopy.

2.5 Measurement of cell proliferation

After an initial overnight incubation, SaOS-2 cells were washed, and the extent of cell proliferation was determined by a 3-(4, 5-dimethylthiazol-2-yl)-2, 5-diphenyltetrazolium bromide (MTT) (Sigma-Aldrich) assay. The cells were washed with PBS, and MTT was diluted using serum-free medium to obtain a concentration of 0.5 mg/mL. This concentration was added to the culture and incubated for 3 h. Formazan extraction was performed using isopropanol, and the quantity was determined using an enzyme linked-immunosorbent assay at 492 nm with four individual samples per group.

2.6 Immunocytochemistry

The same amount of cell suspension was cultured on nine sterilized cover glasses in six well plates. The equal total DMEM media with different sample extracts were added to the corresponding well plates. Cultured for 24 h, the cover glasses were washed three times with PBS to remove non-adherent cells. SaOS-2 cells were fixed 24 h in 4 % paraformaldehyde phosphate buffer solution. Immunocytochemistry staining was performed using antibodies to BMP-2. The signal was developed using a Streptavidin–Biotin complex (SABC) method. Fixed SaOS-2 cells were pretreated with 0.3 % H_2O_2 for 30 min at room temperature to block endogenous peroxidase activity. After washing three times with distilled water, the sections were blocked with 10 % normal goat serum solution for 40 min at room temperature, and then the blocking solution was discarded. The primary antibody (Boster, China) diluted to 0.2 M (1:100) was applied onto the sections, and the sections were incubated at 4 °C for 48 h in a humidified chamber. Following incubation, these were washed three times with 0.1 M PBS for 2 min each and then incubated with the secondary antibody (biotin-goat anti-rabbit IgG BMP-2, Boster, China) diluted to 0.2 M PBS (1:100) for 20 min at 37 °C. The sections were washed three times with PBS for a total 6 min and then exposed to SABC (Boster, China) for 30 min at 37 °C. After rinsing the sections three times at 5 min each, visualization of the antibody staining was accomplished by incubating sections in 0.03 % 3,3-dia-minobenzidine (DAB; Boster, China) for 5 min. The sections were counterstained with hematoxylin. For the controls, the above steps were followed with the primary antibody replaced with PBS. A brown precipitate denotes positive immunostaining.

2.7 Microstructure

To analyze the microstructure of Mg–3AI–1Zn, Ti–6Al–4 V, (β-TCP)–Mg–3AI–1Zn and (β-TCP)–Ti–6Al–4V, samples were removed from the SaOS-2 cell culture, then fixed in 4 % glutaraldehyde for 4 h. The Ti–6Al–4V and (β-TCP)–Ti–6Al–4V were used as control. Samples were dehydrated in ethanol and observed using ssx-550 scanning electronic microscope (SEM). The chemical composition was determined by energy dispersive spectrum (EDS). The area analyzed was determined by random.

2.8 Western blot analysis

SaOS-2 cells were cultured onto the different biomaterial surfaces for 2 h in 25 cm^2 flasks. These were cultured in serum-deprived media, wherein the 10 % serum was replaced with 1 % serum. These were then washed three times with cold phosphate buffer saline (PBS). Cells were lysed and freeze-thawed in RIPA buffer (150 mM NaCl, 50 mM Tris–HCl, pH 7.5, 1 % deoxycholate, 0.1 % SDS, 1 % Triton X-100) containing protease inhibitors (Complete, Roche Diagnostics, Germany). Reduced proteins were resolved by 10 % Tris–HCl polyacrylamide gel

electrophoresis (Bio-Rad Gels) and transferred onto a nitrocellulose membrane (Amersham, Freiburg, Germany). The membranes were blocked overnight in Tris–buffered saline containing 5 % skim milk and 0.05 % Tween-20 (TBST). Shc and c-fos were detected with a rabbit polyclonal antibody (Transduction, 610081) (1:1000), total ERK1/2 was detected with a mouse monoclonal antibody (transduction, 61003) (1:1000), and phosphorylated ERK1/2 was detected with a goat polyclonal antibody (Santa Cruz-7972) (1:1000). Blots were again washed three times with TBST as described above, and immunoreactive bands were visualized using the ECL plus Western blotting detection reagents (Amersham Pharmacia Biotech Inc, Piscataway, NJ, USA). The antibody-bound protein intensities were analyzed using a Chemi-imager-5500 V 2.03 electrophoresis gel image system.

2.9 Statistical analysis

SPSS 16.0 was used to analyze all the statistics. Differences between two groups were analyzed by the separate variance estimation *t* test. Differences among more than two groups were analyzed by an analysis of variance (ANOVA). The statistical significance was defined as $P < 0.05$.

3 Results

3.1 Material properties of (β-TCP)–Mg–3AI–1Zn alloy

Figure 1 shows the surface microstructure and the EDS result of Mg–3AI–1Zn, (β-TCP)–Mg–3AI–1Zn, Ti–6Al–4V and (β-TCP)–Ti–6Al–4V incubated with SaOS-2 cells for 24 h. A porous and netlike surface structure was observed clearly on the surface of the (β-TCP)–Mg–3AI–1Zn. Small cracks were also found on the surface of the Mg–3AI–1Zn, which were due to dehydration during the SEM sample preparation. The EDS analysis on a small area of the alloys, as shown in Fig. 1, indicates that the layer of (β-TCP)–Mg–3AI–1Zn and Mg–3AI–1Zn was mainly composed of O, P, Ca, and Mg. More P and Ca elements were observed on the surface of the (β-TCP)–Mg–3AI–1Zn than of the Mg–3AI–1Zn.

3.2 Morphology of cells grown on (β-TCP)–Mg–3AI–1Zn alloy

SaOS-2 cells cultured for 24 h on Mg–3AI–1Zn, (β-TCP)–Mg–3AI–1Zn, Ti–6Al–4V and (β-TCP)–Ti–6Al–4V were processed for immunofluorescence staining, including

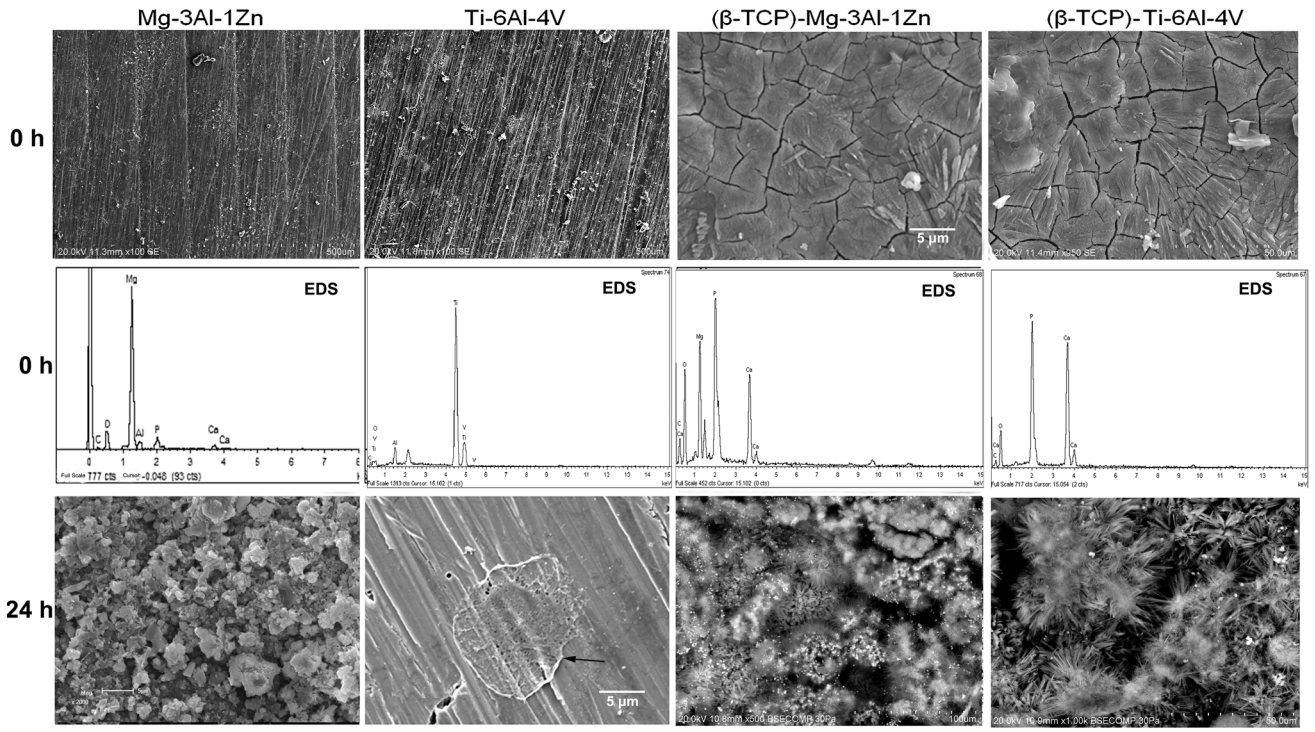

Fig. 1 Surface microstructure (SEM) and EDS results of (β-TCP)–Mg–3AI–1Zn. The Mg–3AI–1Zn, (β-TCP)–Mg–3AI–1Zn, Ti–6Al–4V and (β-TCP)–Ti–6Al–4V alloys were incubated with SaOS-2 cells for 24 h, and then surface structures were analyzed using SEM and EDS

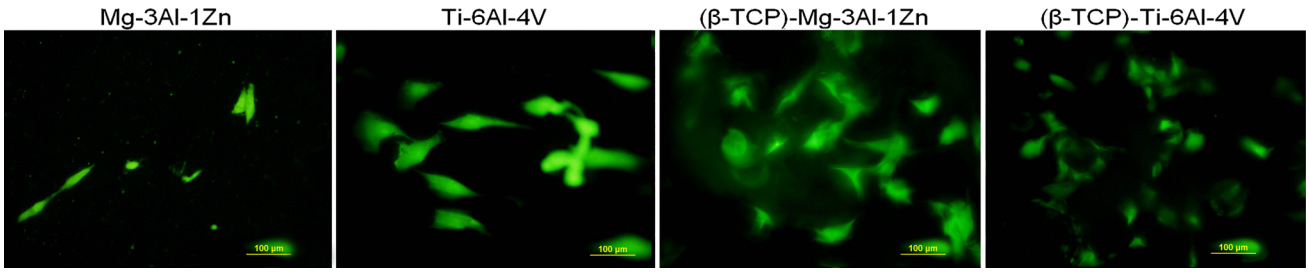

Fig. 2 Scanning electron micrographs of SaOS-2 cells cultured on the alloy surfaces used for immunofluorescence staining. The cells on surfaces were analyzed by immunofluorescence staining

sample preparation, fixed, blocking, primary antibody incubation, secondary antibody incubation, detection of proteins, multiple staining and other steps (Fig. 2). With the Mg–3AI–1Zn, only a few cells were observed on the surface after 24 h of cell culture. With the (β-TCP)–Mg–3AI–1Zn, many cells were observed after only 24 h of cell culture. The cells spread and connected together and covered most of the sample (Fig. 2). The cells displayed a flattened morphology with numerous filamentous extensions. More cells were observed on the surface of the (β-TCP)–Mg–3AI–1Zn than Mg–3AI–1Zn, indicating a better cell response to the (β-TCP)–Mg–3AI–1Zn. With the Ti–6Al–4V and (β-TCP)–Ti–6Al–4 V, the cells were spindle-like and displayed a strong adhesion to the substrate after 24 h culture. A longer duration of the culture incubation did not change the cell morphology. Based on the resulting cell morphology, the (β-TCP)–Mg–3AI–1Zn elicited a better cell response than the Ti–6Al–4V in the 24 h culture because the cells on the surface of the (β-TCP)–Mg–3AI–1Zn spread and connected with each other.

3.3 Effect of (β-TCP)–Mg–3AI–1Zn on cell proliferation

The cell proliferation was determined by MTT assay after the (β-TCP)–Mg–3AI–1Zn was incubated with SaOS-2 cells for 24 h. The cell activity represented by the cell number was found to increase with culture time, indicating that a cell could attach and proliferate on the surface of the samples. With the Mg–3AI–1Zn, we observed a decrease in cell proliferation, indicating that the Mg–3AI–1Zn does not promote cell growth and proliferation. In contrast to the Mg–3AI–1Zn, incubation with (β-TCP)–Mg–3AI–1Zn resulted in a statistically significant increase in cell proliferation at all time intervals ($P < 0.05$) (Fig. 3), indicating that the (β-TCP)–Mg–3AI–1Zn has a significantly better surface bioactivity than the Mg–3AI–1Zn. No statistically significant difference in the cell number between the Mg–3AI–1Zn and the Ti–6Al–4 V was observed.

3.4 BMP-2 is modulated in response to β-TCP coating

In this study, the BMP-2 protein in SaOS-2 cells cultured for 24 h with alloys was determined by immunocytochemistry staining. As shown in Fig. 4, the cells cultured with the Mg–3AI–1Zn exhibited the weakest signal for BMP-2 staining. An elevated level of BMP-2 expression was observed when SaOS-2 cells were cultured with (β-TCP)–Mg–3AI–1Zn. The ability to induce BMP-2 expression by the various samples was as follows: (β-TCP)–Mg–3AI–1Zn > (β-TCP)–Ti–6Al–4V > Ti–6Al–4V > Mg–3AI–1Zn (Fig. 4).

3.5 Levels of Shc and c-fos signaling proteins were enhanced in response to β-TCP coating

SaOS-2 cells cultured for 2 h with Mg–3AI–1Zn, Ti–6Al–4V, (β-TCP)–Ti–6Al–4V or (β-TCP)–Mg–3AI–1Zn were analyzed for levels of specific signaling proteins by western blot. SaOS-2 cells showed a marked increase in the expression of all three Shc isoforms (p66, p52, p46) in SaOS-2 cells cultured with (β-TCP)–Mg–3AI–1Zn (Fig. 5). The order of increased activation of signaling protein was as follows: (β-TCP)–Mg–3AI–1Zn > (β-TCP)–Ti–6Al–4V > Ti–6Al–4V > Mg–3AI–1Zn. As seen in Fig. 5, the extent of activation of c-fos protein in cells was higher with (β-TCP)–Mg–3AI–1Zn than controls.

3.6 β-TCP treatment up-regulated the activation of ERK1/2 in SaOS-2 cells

SaOS-2 cells cultured for 2 h with Mg–3AI–1Zn, Ti–6Al–4V, (β-TCP)–Ti–6Al–4V or (β-TCP)–Mg–3AI–1Zn were analyzed for the activation of ERK1/2 MAP kinase by western blot. As seen in Fig. 6, the level of *p*-ERK1/2 was higher in cells cultured with (β-TCP)–Mg–3AI–1Zn and (β-TCP)–Ti–6Al–4V than in cells cultured with Mg–3AI–1Zn ($P < 0.05$). However, the activation of total ERK1/2

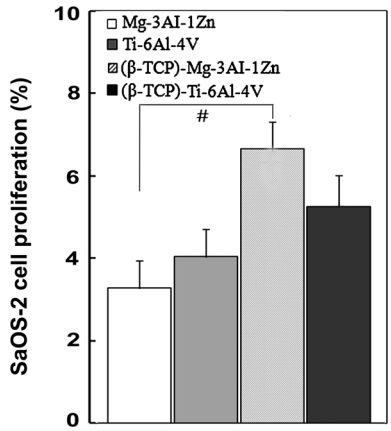

Fig. 3 Effect of different surfaces on cell proliferation. After SaOS-2 cells were incubated with different alloys for 24 h, the cell proliferation was determined by MTT assay. *Hash* shows statistical significance at $P < 0.05$ ($n = 5$), compared with Mg–3AI–1Zn group

MAP kinase did not change in SaOS-2 cells cultured with different alloys.

4 Discussion

Research on Mg alloys as biodegradable materials has been conducted extensively. However, the alkalization caused by the in vivo corrosion of Mg alloys remains a critical obstacle in its possible application as biodegradable implant materials. One way to reduce the corrosion of Mg alloys is surface modification. Mg–3AI–1Zn alloy is likely to degrade the corrosion of naked Mg alloy in aqueous solution, especially in a solution containing chloride ions. In Mg alloys, Al can effectively improve resistance to corrosion and lower the rate of degradation. For biomaterials, a surface coating is an effective surface modification to improve the surface

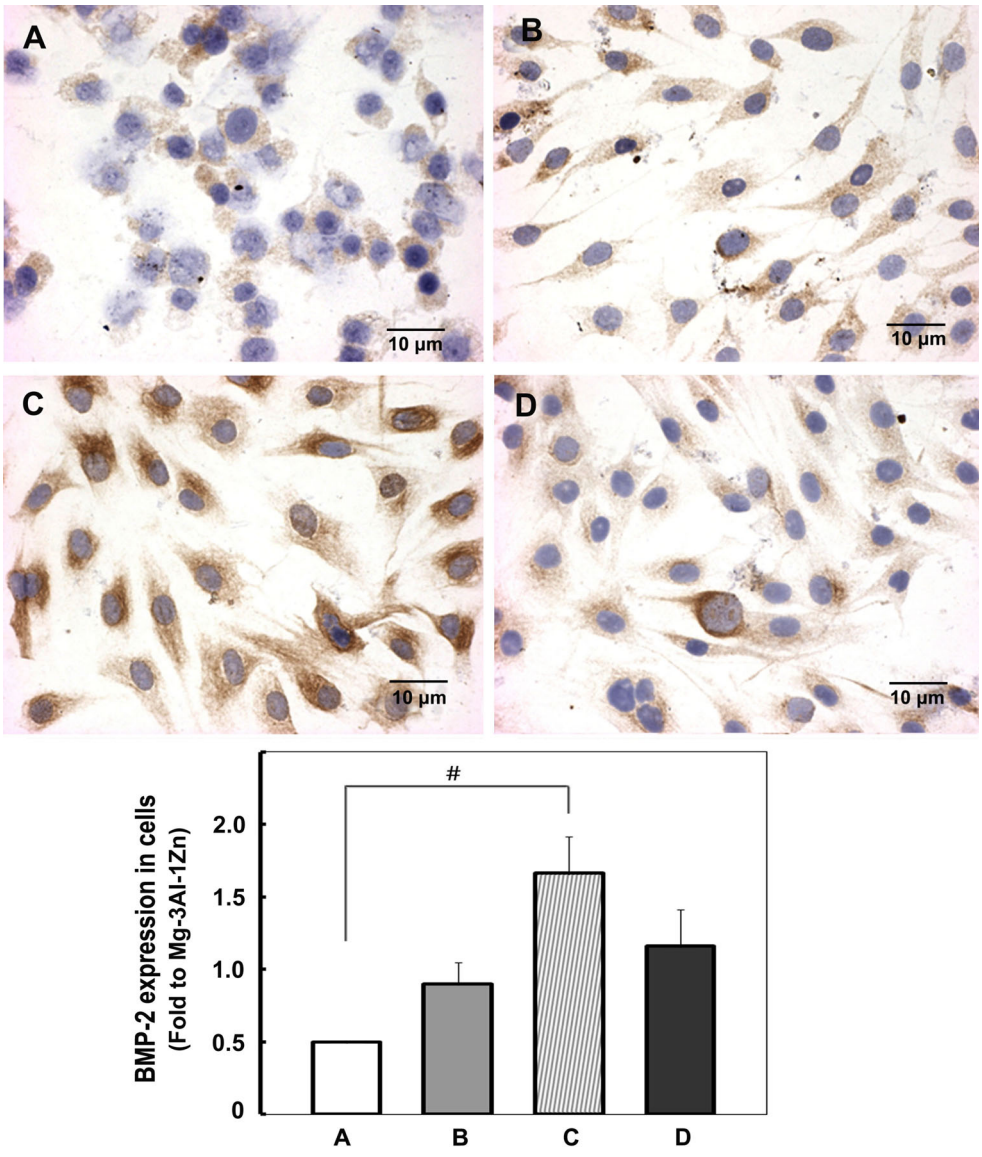

Fig. 4 BMP-2 expression in SaOS-2 cells cultured with different surfaces. The SaOS-2 cells were incubated with different alloys for 24 h. Photomicrographs shown in **a**, **b**, **c** and **d** represent cells cultured with the Mg–3AI–1Zn, Ti–6Al–4V, (β-TCP)–Mg–3AI–1Zn and (β-TCP)–Ti–6Al–4V alloys, respectively. A *brown* precipitate denotes positive immunostaining (Color figure online)

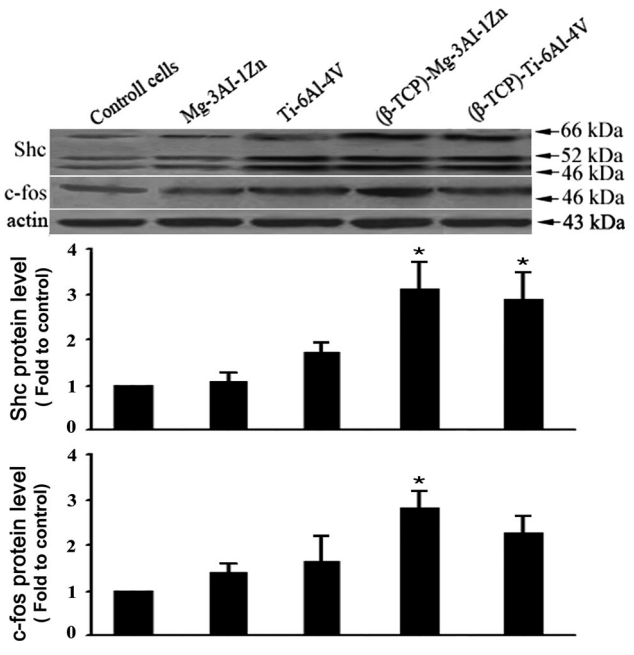

Fig. 5 Effect of β-TCP coating on the expression of Shc and c-fos. Shc expression in SaOS-2 cells cultured for 2 h on control cells with Mg–3AI–1Zn, Ti–6Al–4V, (β-TCP)–Ti–6Al–4V or (β-TCP)–Mg–3AI–1Zn alloys. Equal amounts of total proteins were resolved by 10 % Tris–HCl polyacrylamide gel electrophoresis and analyzed by immunoblotting with anti-Shc and anti-c-fos antibodies. The maximum expression level for the three isoforms (66, 52 and 46) of Shc and c-fos expression was observed when SaOS-2 cells were cultured with alloys. Actin expression served as the loading control

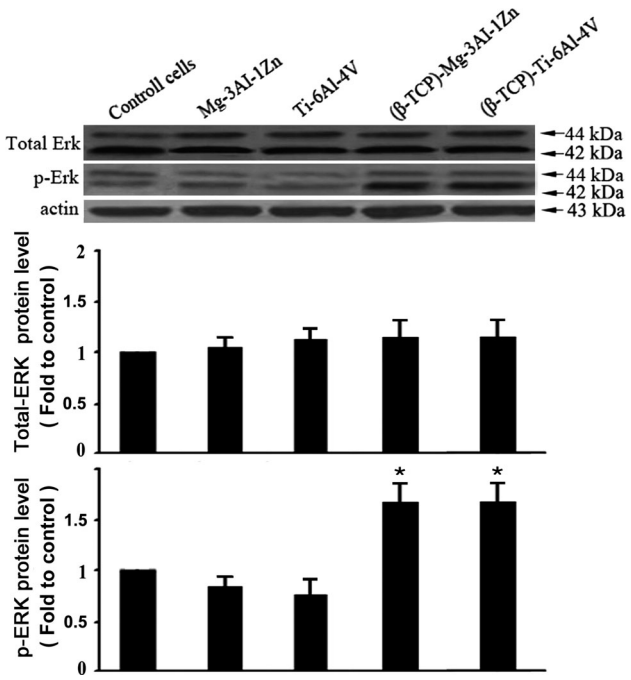

Fig. 6 Total ERK1/2 and phosphorylated ERK1/2 (*p*-ERK1/2) expressed in SaOS-2 cells cultured for 2 h on control cells, with Mg–3AI–1Zn, Ti–6Al–4V, (β-TCP)–Ti–6Al–4V or (β-TCP)–Mg–3AI–1Zn. Immunoreactivity of *p*-ERK1/2 was expressed as a ratio to β-actin. Equal amounts of total protein were resolved by 10 % Tris–HCl polyacrylamide gel electrophoresis and analyzed by immunoblotting with anti-total ERK1/2 and *p*-ERK1/2 antibodies

bioactivity. Therefore, it is possible to reduce the corrosion of Mg alloy and improve its surface bioactivity by selecting a proper surface treatment. This paper is an extension of a previous study in which we successfully showed that surface TCP coating of biomaterials potentiates bone growth in vitro [33]. Because of its chemical similarity to natural bone, β-TCP has been known to be a biocompatible and bioactive material. Despite its biologically favorable properties, TCP cannot withstand the rigors of orthopedic applications. To overcome the problems related to the unfavorable mechanical properties of TCP, coatings have been applied consisting of various metallic substrates. The metallic substrate acts as the load-bearing material, and TCP coating provides a bioactive surface, promoting rapid bony adaptation, reduced healing time and delayed metallic ion diffusion as a biological barrier [34].

The present study introduced the concept of surface treatment coating with β-TCP onto Mg alloy, where we demonstrated the successful surface modification to alter surface characteristics of implants [33]. In this study, the microstructure of the Mg alloy coated with β-TCP shows that the coating layer is porous with a net-like surface structure, as shown in Fig. 1. SEM results indicate that the layer is mainly composed of O, P, Ca, Mg and a little Al. When Mg alloy is immersed in a phosphating bath, Mg dissolves and turns into Mg^{2+}. Mg^{2+} could react with any negative ions in the phosphating bath, such as PO_4^{3-}. The release of calcium ion (Ca^{2+}), PO_4^{3-} and Mg^{2+} might have some effect on cell proliferation and growth [35]. According to the fluorescent images in Fig. 2, more new cells, which are compact and uniform, were observed on the surface of the (β-TCP)–Mg–3AI–1Zn after a 1-day culture, indicating that the (β-TCP)–Mg–3AI–1Zn is more compatible than other coated alloys for bone growth at the early incubation process. These results demonstrate that β-TCP coating improves the surface bioactivity of Mg alloy significantly.

Numerous growth factors have been implicated in the repair of fractures, so the expression of bone growth factors can be used to evaluate osteogenesis at the interface between implant and bone. Among those growth factors, BMP plays crucial roles in normal skeletal development as well as in bone healing, and is able to activate transcription of genes involved in cellular migration, proliferation and differentiation [21–25]. It was reported that endogenous BMP-2 is an indispensable osteogenic stimulus for initiation of fracture healing in mice [27]. Immunocytochemical results revealed that at the early incubation process, the β-TCP coated Mg alloy can induce BMP-2 expression to a level that is significantly higher

than that with the naked Mg alloy after 4 h culture. These results demonstrated that the β-TCP coated Mg alloy has positive effects on osteoblast growth and proliferation in vitro.

We previously found that SaOS-2 cells can bind directly to the implant surface, and the behavior of these cells can be modulated by surface chemistry modification of the underlying substrata [33]. This was in agreement with findings from others [36, 37]. Moreover, Jansen and colleagues [23] reported that BMP-2 promotes osteoblastic differentiation. Processes involving intracellular signalling pathways that connect with the cytoplasmic domains of BMP-2 can result in rapid activation or inactivation of ligand-binding functions, possibly mediated through changes in receptor conformation [38]. Binding of BMP-2 to extracellular matrix proteins results in the activation of signalling pathways in osteoblasts [39]. We showed here that activation of Shc is enhanced when SaOS-2 cells were cultured on the β-TCP modified Mg alloy. Shc, an adaptor protein, is a common point of integration between BMP-2 and Ras/MAPK pathways [40]. Its activation leads to activation of these intracellular signalling pathways [41]. The Ras/MAPK signal transduction pathway is one of the best characterized pathways. Biological studies were conducted to assess the polymer's biological properties, like supporting the cell attachment and proliferation, and inflammation response. The results showed that the bovine aortic endothelial cells had very good attachment and proliferation performance on coating surface [42]. MAPK has been reported to regulate growth and differentiation of bone cells, [29] and its activity is stimulated in osteoblasts when the cells adhere to type I collagen [30, 31]. MAPK acts as an important mediator of the cellular response to various extracellular stimuli [32]. Previous reports indicated that blocking ERK1/2 activation suppresses osteoblast proliferation and differentiation. Once activated, ERK1/2 engages numerous downstream targets, culminating in changes in gene expression and cell behavior [29–31].Our data demonstrate that the level of phosphorylated ERK versus total ERK is increased by osteoblast adhesion to the (β-TCP)–Mg–3AI–1Zn, suggesting that surface chemistry modification of biomaterials modulates osteoblastic cell responses through activation of the ERK/MAPK pathway. This is in agreement with findings from others, in that this pathway modulates osteoblast adhesion to biomaterials [39]. Yamashita et al. [29] demonstrated that ERKs played an important role in outside-in signal transduction regulating osteoblast growth and differentiation. It is also important in inside-in signal transduction modulating integrin levels on the cell surface and consequently, cell adhesion, spreading and migration. Our data demonstrate that surface chemistry modification alters the activation of ERK1/2 in SaOS-2, which may subsequently lead to enhanced bone cell proliferation. AP-1 is one of the most widely studied transcription factors, and c-fos has been implicated as a key molecule in cell proliferation and signal transduction. Our results demonstrated that c-fos expression was induced in SaOS-2 cells cultured on the β-TCP modified Mg alloy. Others have also demonstrated that c-fos expression is associated with osteoblast proliferation in vitro [26–28]. While Mg–3AI–1Zn did not induce any changes in cellular responses under current experimental conditions, further experiments are underway to determine the effect of β-TCP and Mg^{2+} on cell behavior using longer incubation times with the cell cultures and on expression of various proliferative and differentiation markers.

Taken together, the current data suggest that surface chemistry modification of Mg alloy with the bioactive β-TCP is likely to have a role in modulating the extracellular signals in the bone microenvironment, thereby potentially contributing to successful osteoblast function. Further studies are currently underway to understand how different biomaterials and their surface modification elicit distinct signaling pathways in osteoblasts, which may prove beneficial in the design of new implant materials.

Acknowledgments We are thankful to China medical university affiliated hospital laboratory center for kindly providing equipments needed. We thank LetPub (www.letpub.com) for its linguistic assistance during the preparation of this manuscript. This work was supported by the National Natural Science Foundation of China (Grant Numbers 81470998, 81071460, and 81271996).

Conflict of interest The authors have declared that there is no conflict of interest.

References

1. Aghion E, Levy G, Ovadia S. In vivo behavior of biodegradable Mg–Nd–Y–Zr–Ca alloy. J Mater Sci Mater Med. 2012;23(3):805–12.
2. Del Gaudio C, Bagalà P, Venturini M, Grandi C, Parnigotto PP, Bianco A, Montesperelli G. Assessment of in vitro temporal corrosion and cytotoxicity of AZ91D alloy. J Mater Sci Mater Med. 2012;23(10):2553–62.
3. Xu L, Zhang E, Yin D, Zeng S, Yang K. In vitro corrosion behaviour of Mg alloys in a phosphate buffered solution for bone implant application. J Mater Sci Mater Med. 2008;19(3):1017–25.
4. Li ZJ, Gu XN, Lou SQ, Zheng YF. The development of binary Mg–Ca alloys for use as biodegradable materials within bone. Biomaterials. 2008;29(10):1329–44.
5. Kirkland NT, Waterman J, Birbilis N, Dias G, Woodfield TB, Hartshorn RM, Staiger MP. Buffer-regulated biocorrosion of pure magnesium. J Mater Sci Mater Med. 2012;23(2):283–91.
6. Koike M, Hummel SK, Ball JD, Okabe T. Fabrication of titanium removable dental prosthesis frameworks with a 2-step investment coating method. J Prosthet Dent. 2012;107(6):393–9.
7. Rabah MA. Preparation of aluminium–magnesium alloys and some valuable salts from used beverage cans. Waste Manag. 2003;23(2):173–82.
8. Papadopoulos TD, Spyropoulos KD. The effect of a ceramic coating on the cpTi-porcelain bond strength. Dent Mater. 2009;25(2):247–53.

9. Zhang X, Yuan G, Mao L, Niu J, Fu P, Ding W. Effects of extrusion and heat treatment on the mechanical properties and biocorrosion behaviors of a Mg–Nd–Zn–Zr alloy. J Mech Behav Biomed Mater. 2012;7:77–86.
10. Baker MI, Eberhardt AW, Martin DM, McGwin G, Lemons JE. Bone properties surrounding hydroxyapatite-coated custom osseous integrated dental implants. J Biomed Mater Res B Appl Biomater. 2010;95(1):218–24.
11. Kapoor R, Sistla PG, Kumar JM, Raj TA, Srinivas G, Chakraborty J, Sinha MK, Basu D, Pande G. Comparative assessment of structural and biological properties of biomimetically coated hydroxyapatite on alumina (alpha-Al_2O_3) and titanium (Ti–6Al–4V) alloy substrates. J Biomed Mater Res A. 2010;94(3):913–26.
12. Wang C, Karlis GA, Anderson GI, Dunstan CR, Carbone A, Berger G, Ploska U, Zreiqat H. Bone growth is enhanced by novel bioceramic coatings on Ti alloy implants. J Biomed Mater Res A. 2009;90(2):419–28.
13. Taché A, Gan L, Deporter D, Pilliar RM. Effect of surface chemistry on the rate of osseointegration of sintered porous-surfaced Ti–6Al–4V implants. Int J Oral Maxillofac Implants. 2004;19(1):19–29.
14. Hesse C, Hengst M, Kleeberg R, Götze J. Influence of experimental parameters on spatial phase distribution in as-sprayed and incubated hydroxyapatite coatings. J Mater Sci Mater Med. 2008;19(10):3235–41.
15. Toque JA, Herliansyah MK, Hamdi M, Ide-Ektessabi A, Sopyan I. Adhesion failure behavior of sputtered calcium phosphate thin film coatings evaluated using microscratch testing. J Mech Behav Biomed Mater. 2010;3(4):324–30.
16. Shadanbaz S, Dias GJ. Calcium phosphate coatings on magnesium alloys for biomedical applications: a review. Acta Biomater. 2012;8(1):20–30.
17. Xu L, Zhang E, Yang K. Phosphating treatment and corrosion properties of Mg–Mn–Zn alloy for biomedical application. J Mater Sci Mater Med. 2009;20(4):859–67.
18. Leidi M, Dellera F, Mariotti M, Banfi G, Crapanzano C, Albisetti W, Maier JA. Nitric oxide mediates low magnesium inhibition of osteoblast-like cell proliferation. J Nutr Biochem. 2012;23(10):1224–9.
19. Kim YJ, Kim HN, Park EK, Lee BH, Ryoo HM, Kim SY, Kim IS, Stein JL, Lian JB, Stein GS, van Wijnen AJ, Choi JY. The bone-related Zn finger transcription factor Osterix promotes proliferation of mesenchymal cells. Gene. 2006;366(1):145–51.
20. Uauy R, Corvalan C, Dangour AD. Conference on "Multidisciplinary approaches to nutritional problems". Rank Prize Lecture. Global nutrition challenges for optimal health and well-being. Proc Nutr Soc. 2009;68(1):34–42.
21. Liu H, Zhang R, Chen D, Oyajobi BO, Zhao M. Functional redundancy of type II BMP receptor and type IIB activin receptor in BMP2-induced osteoblast differentiation. J Cell Physiol. 2012;227(3):952–63.
22. Tachi K, Takami M, Sato H, Mochizuki A, Zhao B, Miyamoto Y, Tsukasaki H, Inoue T, Shintani S, Koike T, Honda Y, Suzuki O, Baba K, Kamijo R. Enhancement of bone morphogenetic protein-2-induced ectopic bone formation by transforming growth factor-β1. Tissue Eng Part A. 2011;17(5–6):597–606.
23. Van der Zande M, Walboomers XF, Briest A, Springer M, Alava JI, Jansen JA. The effect of combined application of TGFbeta-1, BMP-2, and COLLOSS E on the development of bone marrow derived osteoblast-like cells in vitro. J Biomed Mater Res A. 2008;86(3):788–95.
24. Gonnerman KN, Brown LS, Chu TM. Effects of growth factors on cell migration and alkaline phosphatase release. Biomed Sci Instrum. 2006;42(1):60–5.
25. Zhao L, Yang S, Zhou GQ, Yang J, Ji D, Sabatakos G, Zhu T. Downregulation of cAMP-dependent protein kinase inhibitor gamma is required for BMP-2-induced osteoblastic differentiation. Int J Biochem Cell Biol. 2006;38(12):2064–73.
26. Zanotti S, Canalis E. Nemo-like kinase inhibits osteoblastogenesis by suppressing bone morphogenetic protein and WNT canonical signaling. J Cell Biochem. 2012;113(2):449–56.
27. Kim BG, Lee JH, Yasuda J, Ryoo HM, Cho JY. Phospho-Smad1 modulation by nedd4 E3 ligase in BMP/TGF-β signaling. J Bone Miner Res. 2011;26(7):1411–24.
28. Hou CH, Hou SM, Tang CH. Ultrasound increased BMP-2 expression via PI3K, Akt, c-Fos/c-Jun, and AP-1 pathways in cultured osteoblasts. J Cell Biochem. 2009;106(1):7–15.
29. Yamashita M, Otsuka F, Mukai T, Otani H, Inagaki K, Miyoshi T, Goto J, Yamamura M, Makino H. Simvastatin antagonizes tumor necrosis factor-alpha inhibition of bone morphogenetic proteins-2-induced osteoblast differentiation by regulating Smad signaling and Ras/Rho-mitogen-activated protein kinase pathway. J Endocrinol. 2008;196(3):601–13.
30. Almeida M, Martin-Millan M, Ambrogini E, Bradsher R III, Han L, Chen XD, Roberson PK, Weinstein RS, O'Brien CA, Jilka RL, Manolagas SC. Estrogens attenuate oxidative stress and the differentiation and apoptosis of osteoblasts by DNA-binding-independent actions of the ERalpha. J Bone Miner Res. 2010;25(4):769–81.
31. Weng LP, Smith WM, Brown JL, Eng C. PTEN inhibits insulin-stimulated MEK/MAPK activation and cell growth by blocking IRS-1 phosphorylation and IRS-1/Grb-2/Sos complex formation in a breast cancer model. Hum Mol Genet. 2001;10(6):605–16.
32. Zhu L, Wu Y, Wei H, Xing X, Zhan N, Xiong H, Peng B. IL-17R activation of human periodontal ligament fibroblasts induces IL-23 p19 production: differential involvement of NF-κB versus JNK/AP-1 pathways. Mol Immunol. 2011;48(4):647–56.
33. Chai H, Guo L, Wang X, Gao X, Liu K, Fu Y, Guan J, Tan L, Yang K. In vitro and in vivo evaluations on osteogenesis and biodegradability of a β-tricalcium phosphate coated magnesium alloy. J Biomed Mater Res A. 2011; doi:10.1002/jbm.a.33267.
34. Wang J, de Groot K, van Blitterswijk C, de Boer J. Electrolytic deposition of lithium into calcium phosphate coatings. Dent Mater. 2009;25(3):353–9.
35. Schmitz C, Perraud AL, Johnson CO, Inabe K, Smith MK, Penner R, Kurosaki T, Fleig A, Scharenberg AM. Regulation of vertebrate cellular Mg^{2+} homeostasis by TRPM7. Cell. 2003;114(2):191–200.
36. Fassina L, Visai L, De Angelis MG, Benazzo F, Magenes G. Surface modification of a porous polyurethane through a culture of human osteoblasts and an electromagnetic bioreactor. Technol Health Care. 2007;15(1):33–45.
37. Morra M, Cassinelli C, Cascardo G, Cahalan P, Cahalan L, Fini M, Giardino R. Surface engineering of titanium by collagen immobilization. Surface characterization and in vitro and in vivo studies. Biomaterials. 2003;24(25):4639–54.
38. Kirkbride KC, Townsend TA, Bruinsma MW, Barnett JV, Blobe GC. Bone morphogenetic proteins signal through the transforming growth factor-beta type III receptor. J Biol Chem. 2008;283(12):7628–37.
39. Murakami T, Saito A, Hino S, Kondo S, Kanemoto S, Chihara K, Sekiya H, Tsumagari K, Ochiai K, Yoshinaga K, Saitoh M, Nishimura R, Yoneda T, Kou I, Furuichi T, Ikegawa S, Ikawa M, Okabe M, Wanaka A, Imaizumi K. Signalling mediated by the endoplasmic reticulum stress transducer OASIS is involved in bone formation. Nat Cell Biol. 2009;11(10):1205–11.
40. Zheng Y, Zhao YD, Gibbons M, Abramova T, Chu PY, Ash JD, Cunningham JM, Skapek SX. Tgfbeta signaling directly induces Arf promoter remodeling by a mechanism involving Smads 2/3 and p38 MAPK. J Biol Chem. 2010;285(46):35654–64.
41. Sullivan K, El-Hoss J, Little DG, Schindeler A. JNK inhibitors increase osteogenesis in Nf1-deficient cells. Bone. 2011;49(6):1311–6.
42. Wu J, Chu C-C. Block copolymer of poly(ester amide) and polyesters: synthesis, characterization, and in vitro cellular response. Acta Biomater. 2012;8(12):4314–23.